

Original Research

Characteristic Analysis of Carbon Flux in Paddy Fields in Panjin Wetland

Xudong Zou^{1,2,3*#}, Dawei Zhang^{4#}, Xiyan Yi⁴, Hongli Chen⁴, Rongping Li², Fu Cai^{2**},
Na Mi², Ruiqiang Ding⁵, Xiaoying Wang², Shimin Cao¹, Hujia Zhao²

¹Panjin National Climate Observatory, Panjin 124010, China

²Institute of Atmospheric Environment, CMA, Shenyang 110166, China

³Key Laboratory of Agrometeorological Disasters, Liaoning Province, Shenyang 110166, China

⁴Panjin Meteorological Service, Panjin 124000, China

⁵State Key Laboratory of Earth Surface Processes and Resource Ecology, Beijing Normal University, Beijing 100091, China

Received: 19 August 2024

Accepted: 29 December 2024

Abstract

This study aims to reveal the characteristics of the changes in Net Ecosystem Exchange (NEE) in the rice paddy ecosystem in the Liaohe Plain and its correlation with meteorological factors. Utilizing the observational data from 2020 to 2022 collected at the Panjin Wetland Rice Paddy Agroecosystem Observatory, this study analyzes the changing characteristics of NEE, Gross Primary Productivity (GPP), and Ecosystem Respiration (Reco). The study analyzes the changing characteristics of temperature, precipitation, and wind speed and their correlations and interactions with NEE, GPP, and Reco. Additionally, it calculates the temperature sensitivity parameter for ecosystem respiration (Q_{10}). The research results indicate that the annual total of NEE is negative, indicating a carbon sink. Specifically, NEE is negative during the growing season, representing a carbon sink, while it is positive during the non-growing season, indicating a carbon source. Among the three years, 2021 had the largest total NEE of $-432.89 \text{ gCm}^{-2}\cdot\text{y}^{-1}$. The combination of higher temperatures and more precipitation throughout the year contributed to the high NEE value. The daily variation of NEE first increases and then decreases, with the maximum NEE occurring in July, reaching a range of -20.6 to $-26.0 \mu\text{mol}\cdot\text{m}^{-2}\cdot\text{s}^{-1}$. Temperature, precipitation, sunshine, and specific humidity all contribute to an increase in NEE values, among which temperature has the most significant impact on NEE. During the growing season, NEE significantly increases with rising temperature, reaching its maximum when the temperature is above 30°C , averaging $-8.079 \mu\text{mol}\cdot\text{m}^{-2}\cdot\text{s}^{-1}$. GPP values increased first and then decreased from June to September, with the maximum occurring in July, with a daily cumulative value of 10.69 to $13.55 \text{ gCm}^{-2}\cdot\text{d}^{-1}$. The annual variation of GPP peaks in summer, first increasing and then decreasing. The GPP in July and August accounts for 52.7 to 60.8% of the total annual GPP. There is a quadratic polynomial relationship of negative growth between NEE and net radiation, with the highest correlation value in

*e-mail: 285520084@qq.com

**e-mail: caifu@iaesy.cn

equal contribution

July. During the daytime, NEE increases as net radiation increases but often lags behind the change in net radiation. Reco is the highest in the summer, up to 6.7 times higher than in other seasons. Reco exhibits an exponential relationship with soil temperature, with the highest correlation observed in autumn 2020. In summer, the variability of Reco with soil temperature is higher than in other seasons. The Q_{10} value in summer is the highest, ranging from 2.89 to 6.37, which is 2 to 3 times higher than in other seasons, followed by autumn. In 3a, the Q_{10} values in summer and autumn were the highest in 2021, and the corresponding annual NEE values were also the highest.

Keywords: carbon flux, paddy field, performance characteristics, interaction

Introduction

The Earth is experiencing global warming, and the report of the Intergovernmental Panel on Climate Change (IPCC) [1] points out that the observed land temperature has risen by 1.61°C between 1850–1900 and 2011–2020. Carbon exchange processes are the core content of the material and energy cycle between terrestrial ecosystems and the atmosphere [2]. About one-fifth of the carbon dioxide in the atmosphere comes from the soil, which is more than ten times the amount of man-made carbon dioxide emissions [3]. Any small change in soil respiration will affect the global carbon budget and have a profound impact on global climate change. In the context of the country's goal of achieving carbon peaking and neutrality, conducting research on carbon flux observation is particularly important. The carbon cycle in terrestrial ecosystems is a hotspot in research on global climate change and regional sustainable development. Soil is the largest carbon reservoir in terrestrial ecosystems [4], which has a high level of primary productivity and can lead to high carbon sequestration [5], thus alleviating the trend of global warming to a certain extent [6]. Panjin Wetland is located at Liaohe River Delta's south end, covering an area of over 800 square kilometers. Wetlands play a crucial role in climate regulation and air purification in Liaoning, the entire Northeast region, and even Northeast Asia. GIS spatial analysis revealed that the wetland area in Panjin decreased significantly from 1985 to 2017 [7]. Human activities have caused severe damage to the wetland's ecological environment. Currently, there is limited research on carbon flux in wetland ecological environments, and the future changes in carbon flux and environmental impacts remain unclear [8]. Therefore, it is necessary to conduct observational research on wetland carbon flux.

Currently, scholars from various countries have conducted extensive research on ecosystem carbon flux, mainly focusing on three aspects. First, they studied the characteristics of carbon cycle changes in various types of ecosystems through carbon flux observations and calculations. For example, changes in ecosystem carbon flux in the Great Lakes and surrounding areas of the United States have been studied to quantify the annual trends and patterns of lake carbon output [9, 10]. Study on carbon and water fluxes during the growing season

in three alpine grassland ecosystems in the eastern Tibetan Plateau and control factors of carbon and water fluxes during the growing season in the alpine grassland ecosystem of Nam Co Lake in both dry and wet years [11, 12]. Periodic dynamics of carbon and water fluxes in Shenzhen, China [13]. Lateral transfer of macrodetritus carbon and calculation of gross primary productivity in typical coastal salt marsh wetlands of the Yangtze River Estuary [14]. Dynamic changes and fitting of light response curves for carbon flux in Moso bamboo forests in Zhejiang, China [15]. Multiple analytical methods are used to classify the sources of carbon flux based on observational data [16]. Secondly, apart from eddy covariance observations, satellite observation data are used to invert and estimate the carbon flux budget of large-scale ecosystems. For example, comparing the magnitude and seasonal dynamics of CO_2 flux in winter wheat under conventional tillage and no-tillage management systems in Oklahoma farmland [17]. Contribution of China's forest carbon sequestration to the global environment [18]. Estimating global terrestrial biosphere carbon flux anomalies [19]. Thirdly, establishing simulation models for carbon flux calculation. For example, simultaneously predicting hourly water flux and carbon flux at the point scale or field scale in water-saving irrigated rice fields in the Taihu Lake basin [20]. Use the exponential model to describe the relationship between CO_2 emissions and soil temperature [21].

With a solid theoretical foundation and a wide range of applications, eddy covariance technology is the most effective direct measurement method in flux observation and has been widely used [22]. The wetlands in Panjin have a flat and open terrain, which is relatively suitable for using eddy covariance observation. This study utilizes the carbon flux observation data from the Panjin rice paddy ecosystem station from 2020 to 2022 to analyze the characteristics of rice paddy carbon flux during different periods, investigate the impact of meteorological factors on carbon flux, and calculate the variation characteristics of primary productivity and vegetation respiration.

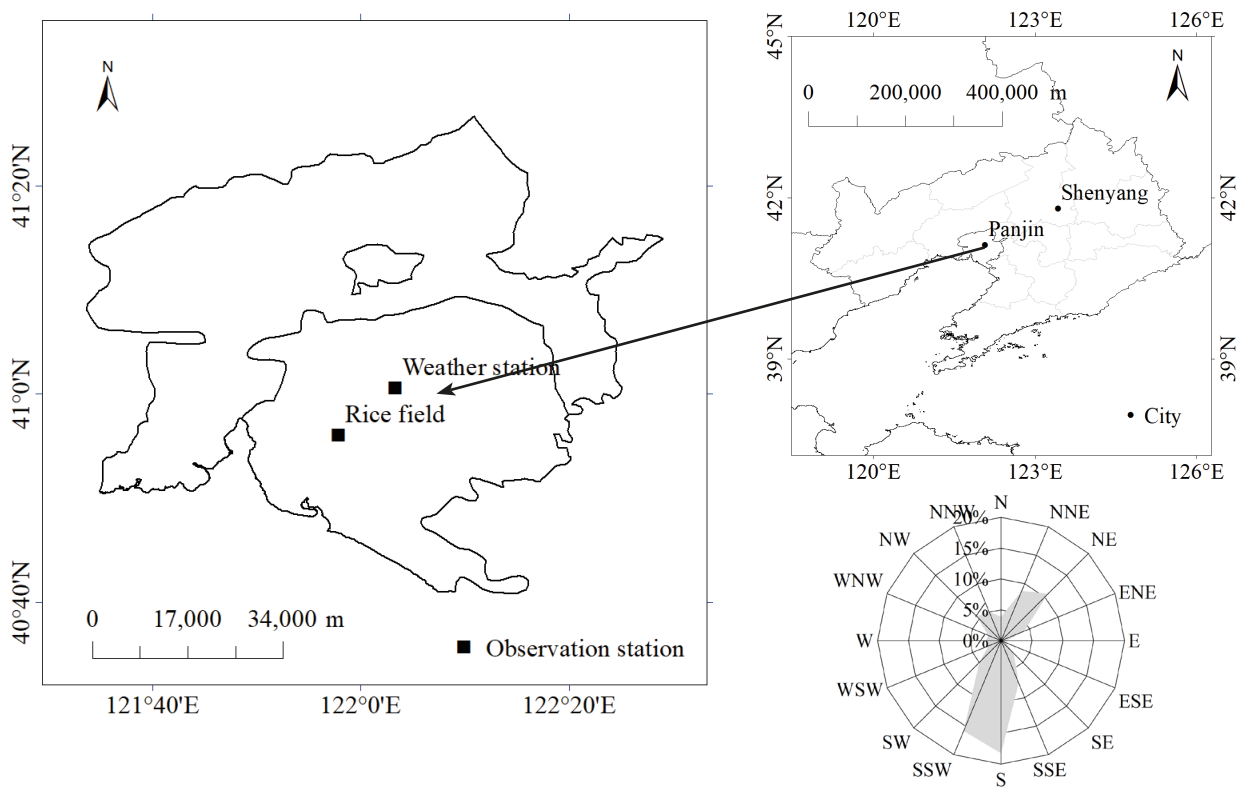


Fig. 1. Location of the study area and the observation site of rice paddies. The wind rose diagram shows the average wind direction at the observation site from 2020 to 2022.

Observations and Methods

Description of the Study Area

The Liaohe River Delta is one of the eight major river deltas in the world, with rich water resources and diverse wetland resources. Panjin Wetland Paddy Field Ecological Observation Station is located in Dawa District, Panjin City, which is Panjin Rice Field Experimental Station (121°57'E, 40°55'N, altitude 4.0 meters) of Shenyang Atmospheric Environment Research Institute of China Meteorological Administration. The observation field covers an area of 25×25 m, and the crop planted is japonica rice. The research area is located north of Bohai Bay, belonging to the continental semi-humid monsoon climate of the north temperate zone, with the rainy and hot seasons in the same period and four distinct seasons. The average annual precipitation is 631 mm, the sunshine duration is 2780 hours, and the annual average temperature is 9.5°C. The highest and lowest temperatures occur in July and January, respectively [23, 24]. Statistically, the dominant surface wind direction from 2020 to 2022 is S, SSW, followed by NE (Fig. 1).

Observation Data and Methods

Collecting carbon flux data for the rice paddy comes from the open-path eddy covariance flux observation system. The observation site is located in an open

and flat area without obstructions from buildings. The ground crops are all rice, and the available area for the experiment is 30 mu (about 2 hectares). The eddy covariance carbon flux observation system consists of a three-dimensional ultrasonic anemometer (CSAT3), an open-path CO₂/H₂O analyzer (Li-7500), an open-path CH₄ analyzer (Li-7700), and a data acquisition unit (Li-7550). The sensors are positioned at a height of 4.2 meters above the ground, with a sampling frequency of 10 Hz. The 30-minute time series data was obtained through data processing using EddyPro (v7.0.9).

The eddy covariance method can directly measure the fluxes of CO₂, CH₄, and other gasses between vegetation and the atmosphere. However, during nights when the atmospheric structure is relatively stable and turbulence is weak, the diffusion of fluxes may not reach the measurement height of the instrument, reducing the accuracy of the measurements. Additionally, open-path eddy covariance systems are susceptible to weather conditions such as rainfall and fog, as their infrared optical paths are exposed. This can lead to anomalous and missing values in the observational data. We identify an anomaly for the anomalous and missing values in the data when the absolute difference between the data at a certain moment and the average data from the previous five moments is greater than five times the variance. Based on the actual conditions at this site and existing related research, the reasonable range of carbon flux values is set to -60 μmol·m⁻²·s⁻¹ to 60 μmol·m⁻²·s⁻¹ [25]. At the same time, linear interpolation is used to

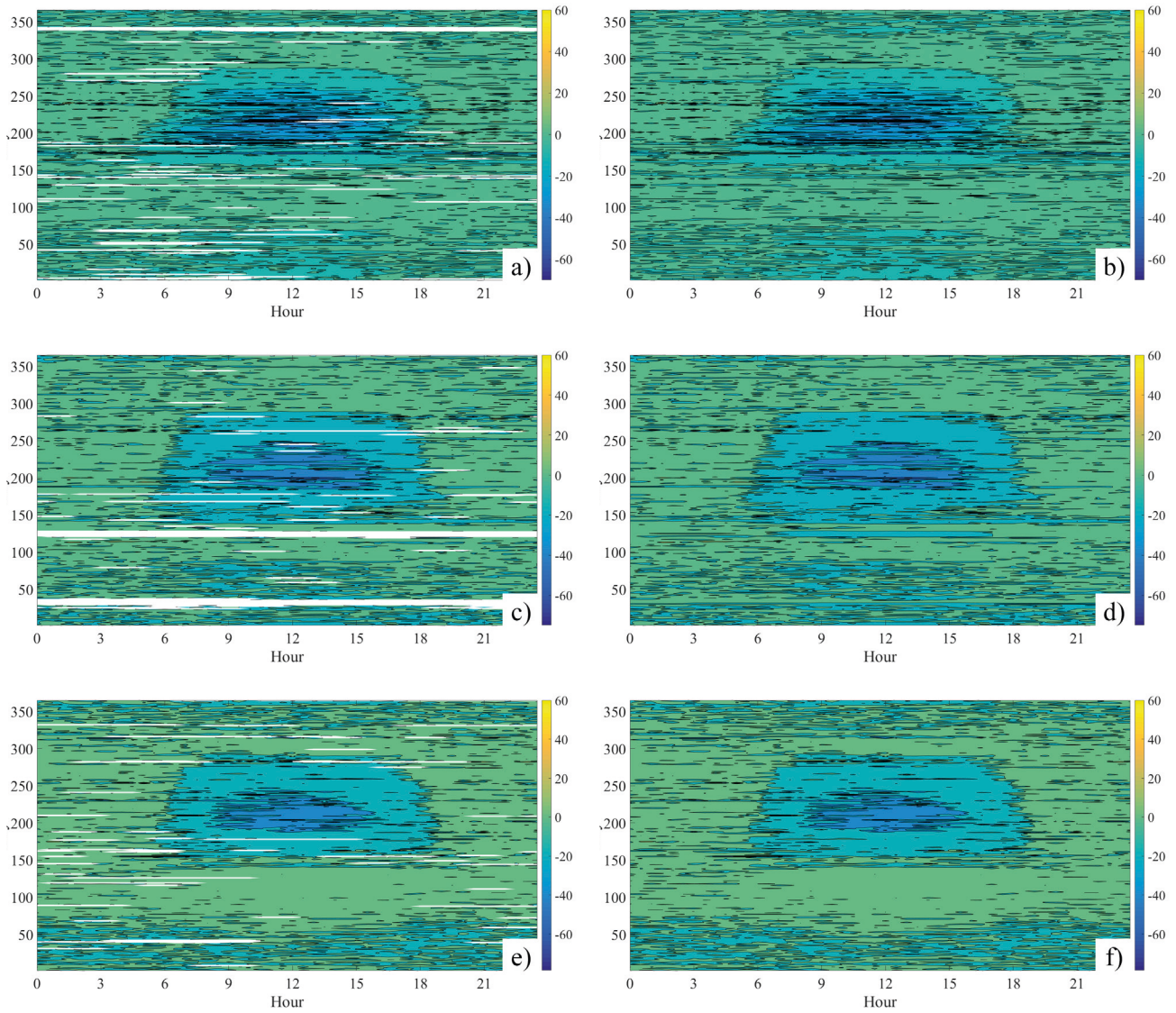


Fig. 2. Description of the missing NEE data by day and hour from 2020 to 2022. The left column (Figure a, Figure c, Figure e) represents the missing data due to power and/or instrument failure or low data quality; the right column (Figure b, Figure d, Figure f) represents the interpolated data.

supplement data gaps of less than 2 hours. For data gaps greater than 2 hours, based on different months, the carbon flux is interpolated separately for daytime and nighttime by establishing relationships between carbon flux and radiation, as well as between carbon flux and ground temperature. When radiation and ground temperature data are also missing, relationships with meteorological factors are established for interpolation. The interpolated data account for 4.8% to 8.3% of the total data volume (Fig. 2). When meteorological data from the ecological station is missing, data from a meteorological station located 11.4 kilometers away is used as a supplement.

Calculation of Ecosystem Parameters

Ecosystem gross primary productivity (GPP) refers to the amount of CO_2 fixed into organic matter by green plants through photosynthesis per unit area and time. Ecosystem respiration (Reco) includes aboveground plant respiration and soil respiration. This process releases most of the carbon fixed by primary productivity in the ecosystem into the atmosphere in the form of CO_2 , which is an important way for the exchange between the soil carbon pool and the atmospheric carbon pool, playing a key role in maintaining the carbon balance of terrestrial ecosystems [26]. The sensitivity of ecosystem respiratory temperature (Q_{10}) refers to the multiple increases in the ecosystem respiration rate when the temperature rises by 10°C , which is used to study the

response of ecosystem respiration to climate change [27]. The specific calculation formula is as follows:

$$GPP = Reco - NEE \quad (1)$$

$$Reco = a \times e^{bT} \quad (2)$$

$$Q_{10} = e^{10b} \quad (3)$$

Where: T is the soil temperature; a and b are coefficients to be determined.

Results and Analysis

Annual Changes in Carbon Fluxes and Meteorological Factors

Meteorological elements are important environmental factors that affect crop growth. Crop growth is very sensitive to changes in meteorological conditions, especially temperature, precipitation, and sunshine duration [28, 29]. From 2020 to 2022, the annual total NEE at the ecological station was negative but was positive during the non-growing season. The growing season was defined as April 16th to October 14th (same below, see Table 1). Among them, the CO₂ absorption value in 2021 was the largest, reaching -432.89 gCm⁻²•y⁻¹, while the carbon absorption values in 2022 and 2020 were lower than -360 gCm⁻²•y⁻¹. The carbon flux during the growing season also showed the largest absorption value in 2021, with 2020 slightly lower than 2022. The variation in carbon absorption during the growing season was up to 79.8 gCm⁻²•y⁻¹, significantly higher than that during the non-growing season. Contrary to the global warming trend, the temperature in the Panjin wetland has decreased in the past three years, while the annual precipitation has been increasing, reaching a maximum of 895.7 mm in 2022. The annual sunshine duration was highest in 2020, reaching 3372.7 hours, which was significantly higher than in 2021 and 2022. The average wind speed was lowest in 2021 and highest in 2022, with a variation of 0.2–0.4 m•s⁻¹. NEE is largest in 2021 in the three-year comparison; the factors that contributed to its promotion were higher temperatures and more precipitation. The

impact of meteorological elements on carbon flux will be analyzed in detail in the following context.

Characterization of Daily Changes in Carbon Fluxes

We respectively calculated the diurnal variation of NEE in spring (March to May), summer (June to August), autumn (September to November), and winter (December and January to February) from 2020 to 2022 (Fig. 3). The seasonal differences in the diurnal variation of NEE are significant. The diurnal variation of NEE in summer and autumn exhibits a "decreasing first and then increasing" pattern, while the variation in winter and spring is less obvious. The daily accumulation of NEE is negative in summer and autumn, which means it acts as a carbon sink. The daily value in summer is much higher than in autumn, with a daily accumulation of -4.28 to -4.82 gCm⁻²•d⁻¹ in summer and -0.35 to -0.61 gCm⁻²•d⁻¹ in autumn. The daily cumulative value in spring and winter is positive, indicating a carbon source.

The diurnal variation of carbon flux in the three months of spring showed obvious differences; sometimes, the value was positive at night and turned negative in the midday of the day. Sometimes, there was no negative value during the day, and the value was positive all day. To describe the characteristics of carbon flux variation in spring in detail, the time periods are divided based on the appearance of significant negative values during the daytime. Each year, significant negative values during the daytime typically occur after late May. The dates when negative values appear in other periods are not fixed. For example, in 2020, negative values appeared in early March, while in 2021, they occurred in early May. In 2022, there were fewer days with negative values. The time when the negative value of carbon flux occurs in Panjin in spring is relatively late, mostly after late May. The main reason is that Panjin is located in the north, with long winters, low temperatures in spring, and a short growing season. The diurnal variation of carbon flux in summer remains relatively consistent over many years. At 6:00 am, with the increase in solar radiation, the photosynthesis of vegetation is enhanced, and the amount of CO₂ absorbed by photosynthesis exceeds the amount released by the ground. At this time, the amount of CO₂ on the ground

Table 1. Annual temperature, precipitation, sunshine, wind speed, and NEE.

Year	T (Annual average) / °C	Annual precipitation P / mm	Sunlight / h	Wind speed / (m•s-1)	Net ecosystem exchange / gCm-2•y-1
2020	10.60	515.7	3372.7	2.62	-359.642 (-433.432 / 73.790)
2021	10.55	769.0	2233.7	2.42	-432.890 (-513.241 / 80.351)
2022	10.33	895.7	2426.8	2.84	-357.198 (-446.632 / 89.435)

Note: "/" means "growing season / non-growing season".

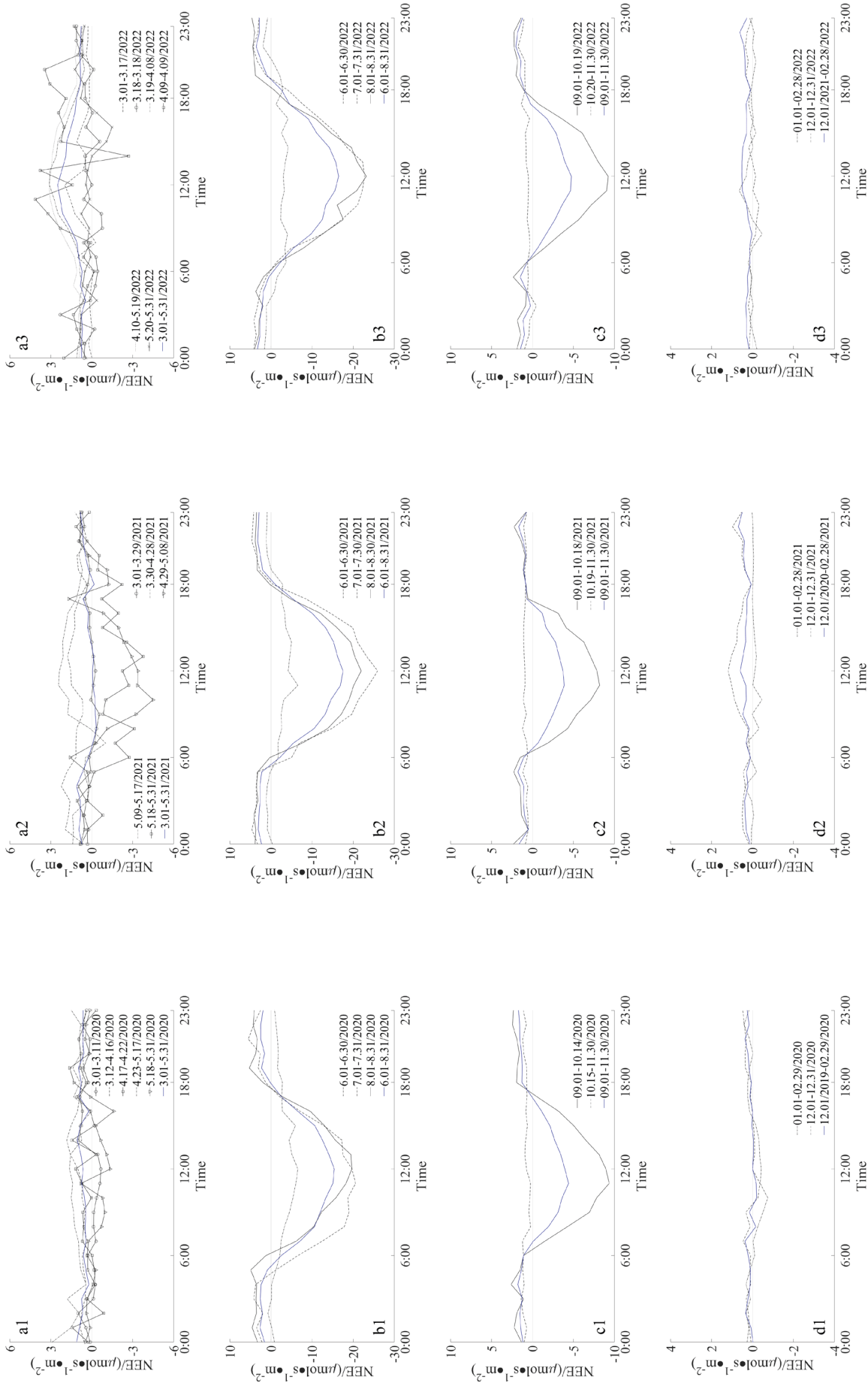


Fig. 3. Average diurnal variation of NEE in different seasons from 2020 to 2022. The NEE value ($\mu\text{mol}\cdot\text{m}^{-2}\cdot\text{s}^{-1}$) represents the average hourly value of carbon flux in the paddy fields in Panjin within the specified date range. Among them, Spring: Figures a1-a3; Summer: Figures b1-b3; Autumn: Figures c1-c3; Winter: Figures d1-d3.

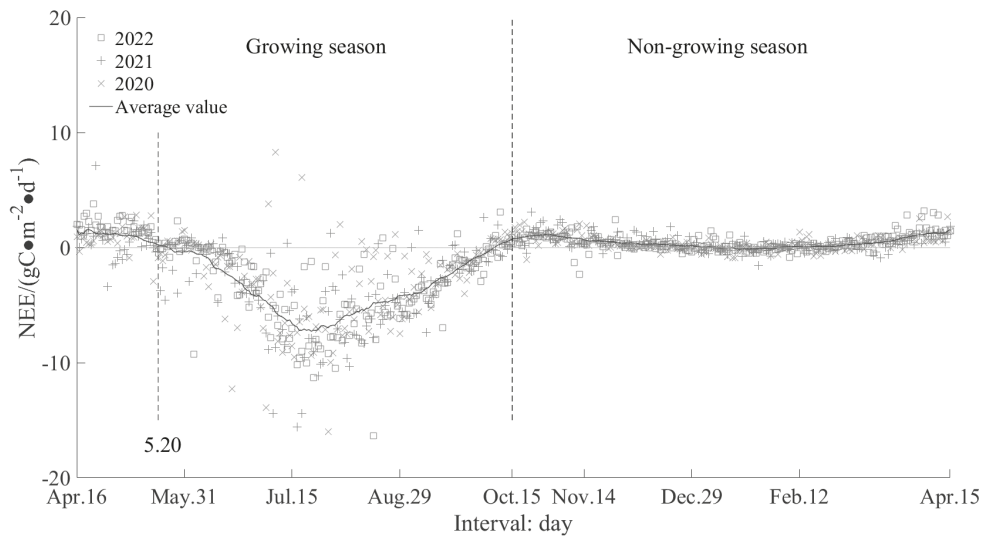


Fig. 4. Comparison of Daily NEE Values in the Growing and Non-Growing Seasons of Panjin Paddy Fields from 2020 to 2022.

surface is converted from release to absorption, and NEE is converted from positive to negative. The carbon absorption reaches its maximum at 12:00 noon. At 18:00 in the evening, NEE changes from negative to positive, and the ground surface changes from carbon absorption to carbon emission. In July, the negative value of NEE is the largest, reaching -20.6 to $-26.0 \mu\text{mol}\cdot\text{m}^{-2}\cdot\text{s}^{-1}$, slightly lower in August than in July and smaller in June.

After mid-October in autumn, there were no significant negative NEE values, and the dates varied slightly each year. In 2020, the date was earlier, on October 15th, while in 2022, it was later, on October 20th. In 2021, it was October 19th. The NEE value turned from positive to negative at 7:00 am and from negative to positive at 17:00 pm, one hour later and earlier than in summer. The maximum carbon absorption occurred at 11:00 or 12:00, reaching -8.2 to $-9.4 \mu\text{mol}\cdot\text{m}^{-2}\cdot\text{s}^{-1}$. During the entire winter, the negative values of NEE during the daytime were relatively small. NEE turned negative from 8:00 to 9:00 am and positive at 16:00 pm. The maximum value occurred between 11:00 and 13:00, ranging from -0.2 to $-0.4 \mu\text{mol}\cdot\text{m}^{-2}\cdot\text{s}^{-1}$.

Statistics on the annual variation of daily carbon flux over a three-year period have been conducted (Fig. 4). Centered on summer, the distribution of the daily value of NEE throughout the year shows a "decreasing first and then increasing" pattern. However, the daily cumulative value of NEE did not show a negative value starting from April 16th, the beginning of the growing season, and only after May 20th did the daily value of NEE turn negative. After October 15th, the daily value of NEE shifted from negative to near zero. It is worth noting that from April to mid-May, the positive value of NEE was slightly higher, indicating that during this period, the crop's aerobic respiration was stronger, but photosynthesis was weaker. This feature was also observed in late October and early November but was weaker than in the spring. The maximum daily

cumulative value of NEE occurs in the middle and late July, ranging from -11.3 to $-16.0 \text{gCm}^{-2}\cdot\text{d}^{-1}$.

Relationship between NEE and Meteorological Factors

Sunshine, temperature, precipitation, etc., are very important natural conditions for the growth of surface vegetation, and the total amount of precipitation and the time distribution of precipitation in the growing season determine the size and duration of the net carbon absorption function of the ecosystem [30, 31]. Fig. 5 shows the daily variation comparison of NEE, precipitation, temperature, sunshine, and other meteorological factors during the active period of carbon absorption (from May 20th to October 14th). NEE reached its maximum in late July, and during the period of high NEE values in summer, the daily variation was relatively large, with a difference between the high and low values ranging from 16.65 to 24.30 $\text{gCm}^{-2}\cdot\text{d}^{-1}$. Precipitation was high in early 2021; for example, it exceeded 75 mm on June 10th and June 27th, but it was low from late July to early August and then increased again in the later period. The precipitation was low in early 2022 but increased significantly in late July and then decreased again afterward. Although the total precipitation in 2022 was the largest, the NEE value was the highest in 2021, indicating that the effect of early-season precipitation on carbon flux was greater than the annual precipitation. The distribution performance of temperature change and NEE are in the opposite phase. The peak values from late July to early August correspond to high values of NEE. From July 23rd to August 1st, 2020, when NEE exceeded $-9 \text{gCm}^{-2}\cdot\text{d}^{-1}$, the daily temperature was higher than 26.7°C . From July 24th to August 8th, 2021, when NEE exceeded $-9 \text{gCm}^{-2}\cdot\text{d}^{-1}$, the daily temperature was higher than 26.0°C . And from July 18th to August 2nd, 2022, when NEE exceeded

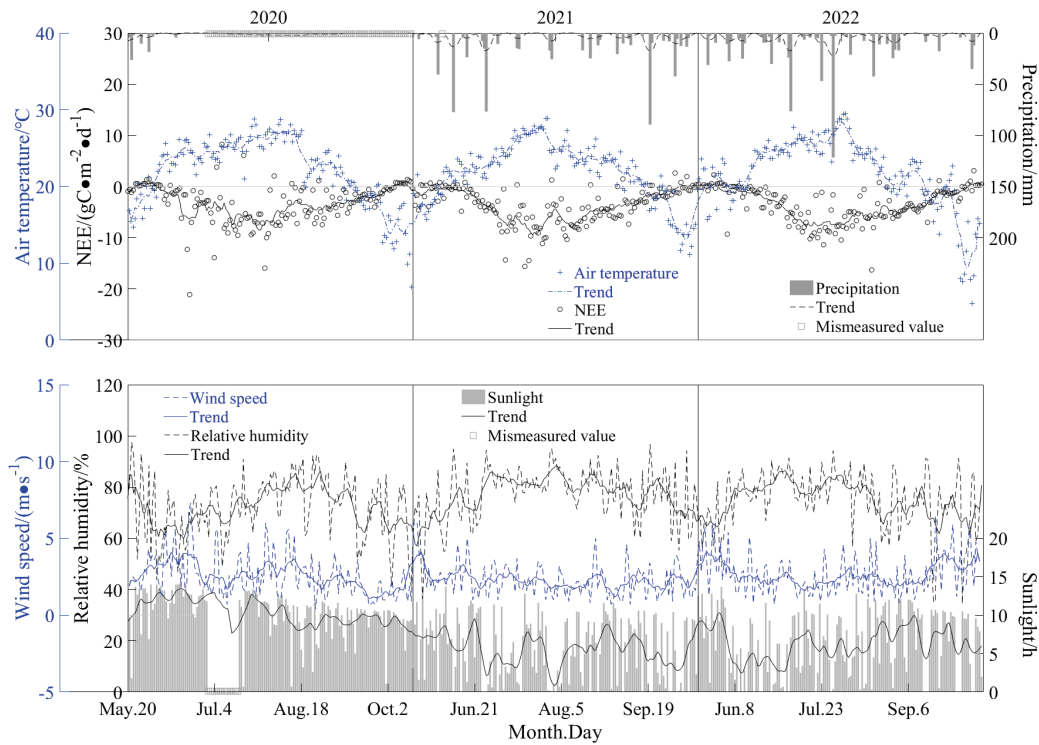


Fig. 5. Comparison of Daily NEE Values ($\text{gCm}^{-2}\cdot\text{d}^{-1}$) in Panjin Paddy Fields from May 20th to October 14th Each Year from 2020 to 2022 with Changes in Daily Values of Precipitation (mm), Temperature ($^{\circ}\text{C}$), Wind Speed (m/s), Specific Humidity (100%), and Sunshine Duration (h).

$-9 \text{ gCm}^{-2}\cdot\text{d}^{-1}$, the daily temperature was higher than 26.1°C . When the temperature is low, the corresponding NEE is also low.

The variation of specific humidity is similar to temperature, and the corresponding specific humidity is larger when precipitation and temperature are higher, but the variation range is lower than that of temperature. Sometimes, high NEE values occur even when the temperature is not particularly high but the specific humidity is relatively large. For example, on July 17, 21, and 24, 2022, the specific humidity exceeded 79.5%, and the NEE value exceeded $-10.0 \text{ gCm}^{-2}\cdot\text{d}^{-1}$, while the daily temperature was below 24.3°C . The variation pattern of wind speed is not significant. The average wind speed in July over the three years ranged from 2.14 to 2.60 m/s, while the average wind speed in September ranged from 1.91 to 2.87 m/s. The wind speed characteristics are not significant when the NEE value is high. The average wind speed from July 15th to August 15th, 2020, is 3.02 m/s, and the average wind speed is 3.82 m/s when NEE is greater than $-9 \text{ gCm}^{-2}\cdot\text{d}^{-1}$. The average wind speed from July 15th to August 15th, 2021, is 1.99 m/s, and the average wind speed is 2.21 m/s when NEE is greater than $-9 \text{ gCm}^{-2}\cdot\text{d}^{-1}$. The average wind speed from July 15th to August 15th, 2022, is 2.27 m/s, and the average wind speed is 1.64 m/s when NEE is greater than $-9 \text{ gCm}^{-2}\cdot\text{d}^{-1}$. It can be seen that the correspondence between wind speed and high values of NEE is not significant. The sunshine value corresponding to the high value of NEE is also high. For example, from July 15th to August

15th, 2021, the average sunshine duration was 5.27 hours, and the average sunshine duration when NEE was higher than $-8 \text{ gCm}^{-2}\cdot\text{d}^{-1}$ was 9.02 hours. From July 15th to August 15th, 2022, the average sunshine duration was 5.52 hours, and the average sunshine duration when NEE was higher than $-8 \text{ gCm}^{-2}\cdot\text{d}^{-1}$ was 7.43 hours. The slightly lower sunshine values were due to precipitation on 3 days.

Temperature, precipitation, sunshine, and specific humidity all promote NEE. Among several meteorological factors, temperature has the most significant correspondence with changes in NEE over a long period, followed by precipitation and specific humidity. The main reason for the high carbon absorption value in the growing period in 2021 was the higher precipitation in the early stage and the higher temperature in the later stage of 2021.

The NEE values were compared between the growing and non-growing seasons for temperature ranges of $15\text{--}30^{\circ}\text{C}$ with an interval of 5°C over a period of 3 years (Table 2). In the non-growing season, temperatures below 15°C accounted for the majority, reaching up to 96.15%, while the remaining only accounted for 3.85%. The NEE values for all temperature ranges during the non-growing season were positive, indicating carbon release. During the growing season, the proportion of temperatures below 15°C was 15.79%, with the highest proportion of 36.38% falling between $20\text{--}25^{\circ}\text{C}$, and the lowest proportion of 2.42% above 30°C .

Table 2. The mean concentration of NEE at different air temperatures from 2020 to 2022.

Temperature $t/^\circ\text{C}$	Monitoring hours / h	Proportion / %	Mean value of NEE / ($\mu\text{mol}\cdot\text{m}^{-2}\cdot\text{s}^{-1}$)
$t \leq 15$	2069 / 12692	15.79 / 96.15	0.454 / 0.398
$15 < t \leq 20$	2974 / 443	22.70 / 3.36	-0.300 / 1.013
$20 < t \leq 25$	4767 / 59	36.38 / 0.45	-2.660 / 1.253
$25 < t \leq 30$	2977 / 6	22.72 / 0.05	-5.400 / 1.341
$30 < t$	317 / 0	2.42 / 0	-8.079 / -

Note: "/" means "growing season / non-growing season".

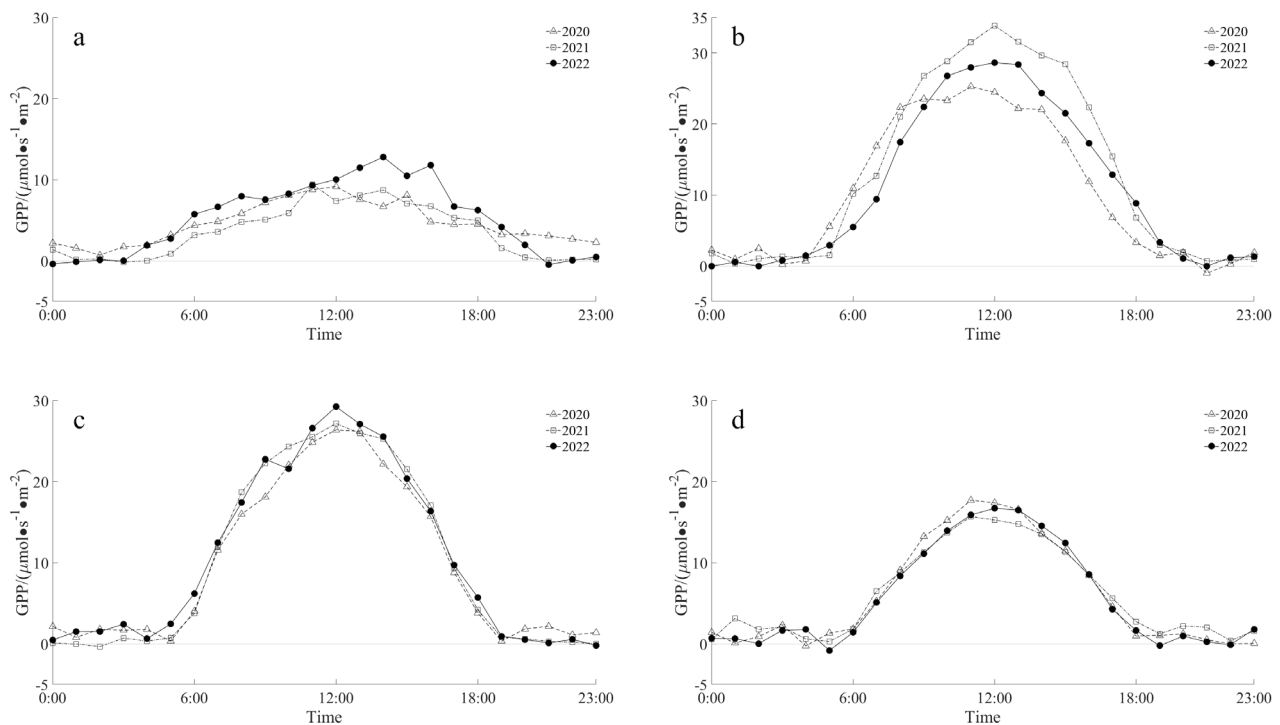


Fig. 6. Comparison of daily variations in hourly GPP ($\mu\text{mol}\cdot\text{s}^{-1}\cdot\text{m}^{-2}$) values in rice paddies in Panjin from 2020 to 2022 in different months, with Figures a-d representing June to September, respectively.

During the growing season, when the temperature is below 15°C , the NEE value is positive, similar to the non-growing season. However, the NEE values are negative for other temperature ranges, indicating carbon absorption. The NEE value increased significantly with the rise of temperature during the growth season, and the mean value of NEE was the largest at $-8.079 \mu\text{mol}\cdot\text{m}^{-2}\cdot\text{s}^{-1}$ when the temperature was higher than 30°C . It is worth noting that the mean value of NEE increased similarly when the temperature rose by 5°C within the range of 15°C to over 30°C , specifically, -2.36 , -2.74 , and $-2.68 \mu\text{mol}\cdot\text{m}^{-2}\cdot\text{s}^{-1}$.

Characteristics of Daily Changes in GPP

The hourly daily changes of GPP from June to September of 2020–2022, which are the months when

crops grow most vigorously and concentratedly, were counted respectively (Fig. 6). The diurnal variation of GPP was significantly different in each month. The diurnal variations from June to September all exhibit a pattern of "increasing first and then decreasing", with June being less prominent. The GPP value was the highest in July, with an average daily accumulation of $10.69\text{--}13.55 \text{ gCm}^{-2}\cdot\text{d}^{-1}$, followed by August, with an average daily accumulation of $10.13\text{--}10.89 \text{ gCm}^{-2}\cdot\text{d}^{-1}$, and the lowest in June, ranging from $3.68\text{--}5.43 \text{ gCm}^{-2}\cdot\text{d}^{-1}$. The months of July and August in summer are the hottest and most humid periods of the year, when the photosynthesis capacity of crops is the strongest, leading to the highest proportion of gross primary productivity. According to statistics, the total GPP in July accounts for $28.6\text{--}31.1\%$ of the annual total, while August accounts for $24.1\text{--}29.7\%$. The total GPP for July

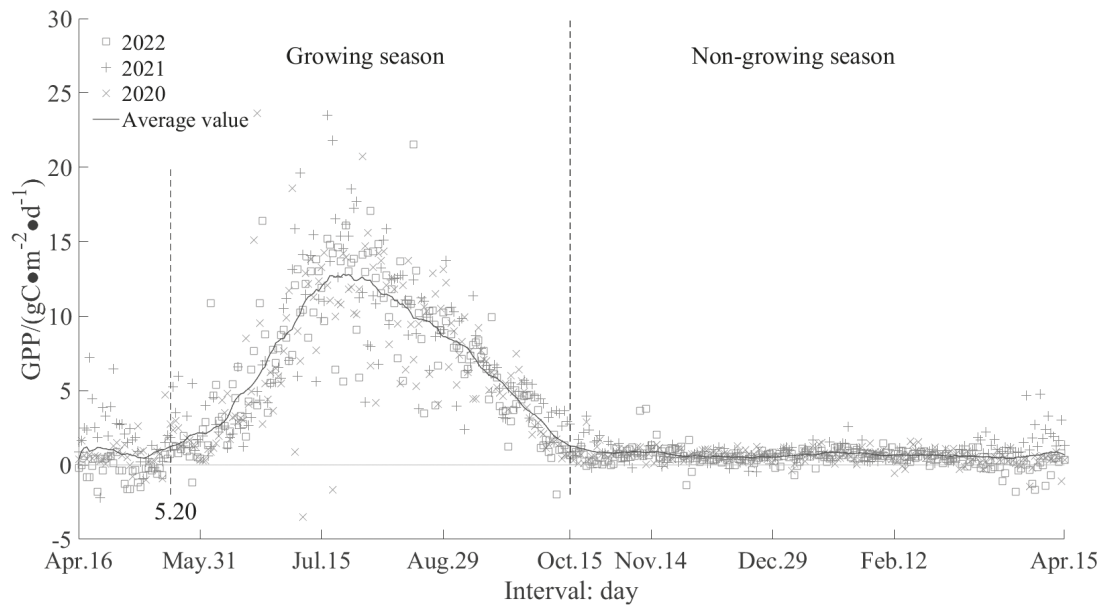


Fig. 7. Comparison of daily GPP ($\text{gC}\cdot\text{m}^{-2}\cdot\text{d}^{-1}$) changes in Panjin rice paddies during the growing and non-growing seasons from 2020 to 2022.

and August accounts for 52.7–60.8% of the annual total. During the diurnal variation, the GPP value gradually increases starting at 5:00, reaches its peak around 12:00 noon, and then begins to decline, falling to a low value between 19:00 and 20:00. The interannual differences in GPP's nighttime variation are relatively small, while the diurnal variation differences are significant. Among them, the diurnal variation in July is the most significant, with the diurnal variation in July 2021 being higher than in other years. Correspondingly, the total GPP in 2021 was also the highest.

In the annual variation of daily GPP values (Fig. 7), the trend is "increasing first and then decreasing", centered on summer. The high values appear from late July to early August, with the maximum daily value ranging from 20.75 to 23.51 $\text{gC}\cdot\text{m}^{-2}\cdot\text{d}^{-1}$. Starting from May 20th, the daily GPP value gradually increases, with the average value reaching its maximum on July 23rd and declining continuously, dropping to a low value by October 15th. In the early growing season, from April 16th to May 20th, the total primary productivity of crops was relatively low, with an average GPP of 0.35–1.23 $\text{gC}\cdot\text{m}^{-2}\cdot\text{d}^{-1}$. After October 15th, the GPP value remained at a relatively low level, averaging 0.68 $\text{gC}\cdot\text{m}^{-2}\cdot\text{d}^{-1}$.

Relationship between Carbon Fluxes and Net Radiation

Solar shortwave radiation is the main energy source of the atmosphere, and net radiation is the main controlling factor for the diurnal variation of NEE in the growing season. We have statistically analyzed the correlation between the diurnal variations of NEE and net radiation from June to September 2020–2022 (Fig. 8). The relationship between NEE and net radiation is a quadratic polynomial with negative growth. From July

to September, the correlation values between the two variables are relatively high, with the highest correlation value occurring in July, where the R^2 of each year is above 0.98. In June, however, the correlation values are lower, with R^2 ranging from 0.64 to 0.83. During the day, when net radiation is greater than 0, NEE is negative, indicating that the vegetation absorbs CO_2 through photosynthesis. At night, when net radiation is less than 0, NEE becomes positive, indicating that the vegetation releases CO_2 through aerobic respiration. These two processes alternate. Starting at 6:00 in July, net radiation turned positive (ranging from 7.2 to 50.3 W/m^2), indicating that photosynthesis in the vegetation exceeded respiration, switching from releasing CO_2 to absorbing it. The NEE value ranges from -1.21 to -6.54 $\mu\text{mol}\cdot\text{m}^{-2}\cdot\text{s}^{-1}$. After that, as net radiation increases, the ability of vegetation to absorb CO_2 gradually enhances, and the NEE value also increases, reaching a peak between 11:00 and 12:00. At this time, the net radiation value is 370.78–382.83 W/m^2 , and the NEE value is -20.57 to -25.95 $\mu\text{mol}\cdot\text{m}^{-2}\cdot\text{s}^{-1}$. Then it begins to decline, and at 18:00, net radiation turns negative, and NEE turns positive between 18:00 and 19:00. The variation of NEE is sometimes lagging behind and sometimes ahead of net radiation, with most of the time lagging behind and sometimes ahead in the morning. For example, in August 2021, the peak of net radiation appeared at 11:00 (310.26 W/m^2), while the peak of NEE appeared at 12:00 noon (-21.94 $\mu\text{mol}\cdot\text{m}^{-2}\cdot\text{s}^{-1}$). In August 2022, net radiation turned positive at 7:00 (64.75 W/m^2), and NEE turned negative at 6:00 (-1.75 $\mu\text{mol}\cdot\text{m}^{-2}\cdot\text{s}^{-1}$).

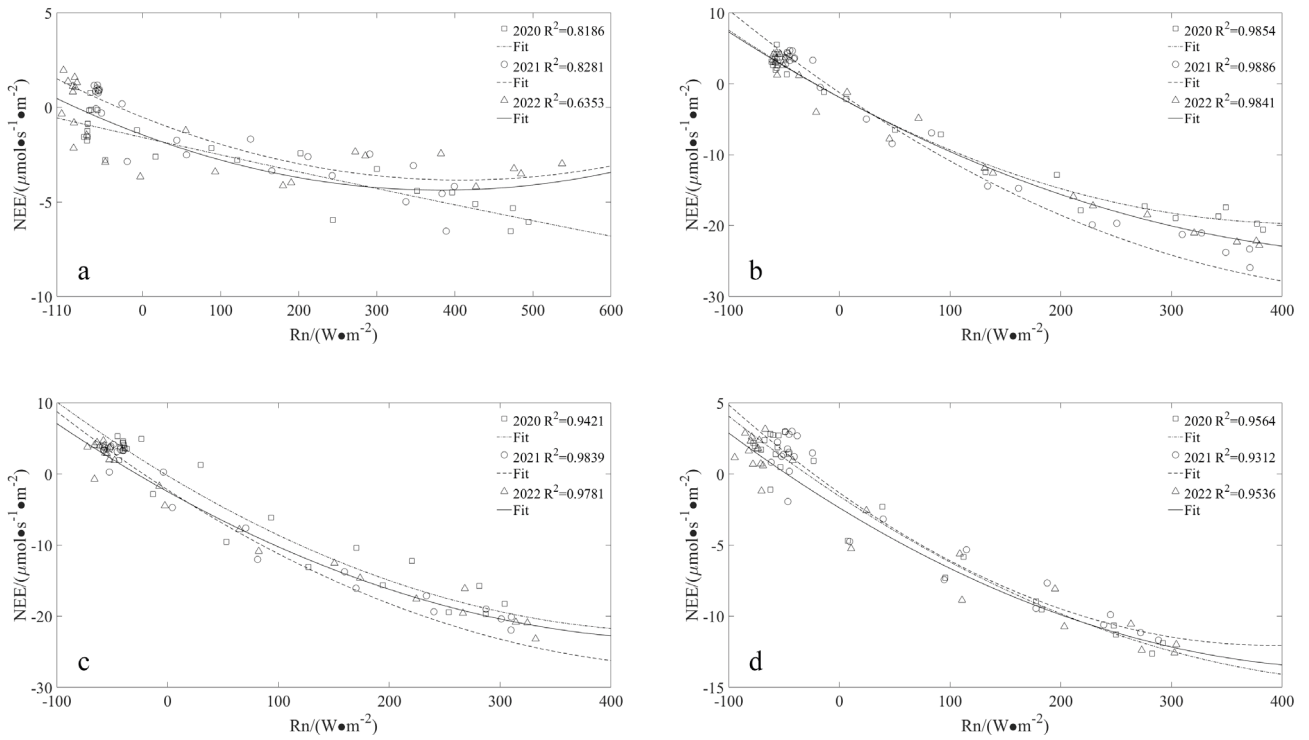


Fig. 8. Corresponding relationship between net radiation (W/m^2) and NEE ($\mu mol \cdot m^{-2} \cdot s^{-1}$). The symbols of triangle, square, and plus represent the corresponding values of the two in different years, and the curve represents the quadratic polynomial relationship between the two. Figures a-d represent the period from June to September.

Ecosystem Respiration (Reco) as Affected by Soil Temperature

Soil temperature is crucial for ecosystem respiration. The study pointed out that when precipitation is no longer a limiting factor for vegetation growth, temperature has a greater impact on plant respiration [32, 33]. There is a clear exponential relationship between the two (Fig. 9), where Reco increases with the rise in soil temperature. The correlation between Reco and soil temperature in each season is significant, passing the 0.01 correlation test. Among them, the respiratory intensity of summer crops was relatively high, ranging from 4.54 to 5.68 $gCm^{-2} \cdot d^{-1}$, with the highest respiratory intensity in the summer of 2020 reaching 5.68 $gCm^{-2} \cdot d^{-1}$. Respiratory intensity in summer is 0.7 to 6.7 times higher than in other seasons; autumn is 0.4 to 2.6 times higher than spring and winter, and winter has the weakest respiratory intensity.

The amplitude of the respiratory intensity of summer crops with soil temperature is higher than in other seasons. The variation of summer ground temperature in the three years ranged from 18.2 to 29.7°C, and the variation of Reco ranged from 1.1 to 11.4 $gCm^{-2} \cdot d^{-1}$. For every 1°C increase in soil temperature, the respiratory intensity increased by 0.71 to 0.85 $gCm^{-2} \cdot d^{-1}$. The maximum increase in Reco with soil temperature occurred in 2022, reaching 0.85 $gCm^{-2} \cdot d^{-1}$. In autumn, the increase in Reco per 1°C rise in soil temperature ranges from 0.13 to 0.22 $gCm^{-2} \cdot d^{-1}$. In spring, the

increment of Reco per 1°C rise in soil temperature ranges from 0.07 to 0.13 $gCm^{-2} \cdot d^{-1}$. In winter, the increment of Reco per 1°C rise in soil temperature is only 0.05 to 0.08 $gCm^{-2} \cdot d^{-1}$.

In the exponential correlation between Reco and soil temperature, autumn exhibited the highest correlation values in 2020–2022, followed by summer, spring, and winter in descending order (see Table 3). The highest correlation value in autumn ($R^2=0.85$) was observed in 2020, while the highest correlation value in summer ($R^2=0.69$) was recorded in 2022. Q_{10} is an important parameter that shows the interaction between terrestrial ecosystems and climate systems. The characteristics of Q_{10} and respiration can help us better understand the interaction between climate change and the carbon cycle of terrestrial ecosystems [34, 35]. The magnitude of Q_{10} depends on the variation of Reco with soil temperature. When Reco varies more significantly with soil temperature, the Q_{10} value increases. During the three-year observation, Q_{10} was highest in summer, ranging from 2.89 to 6.37, followed by autumn with values between 1.67 and 1.91. Both spring and winter showed lower Q_{10} values than autumn. The Q_{10} value in summer is 2 to 3 times higher than in other seasons, indicating that NEE, GPP, and Reco of the ecosystem are at high levels in summer, and the temperature sensitivity of crop respiration is also the strongest. In summer and autumn, the Q_{10} values in 2021 were the highest, 6.37 and 1.91, respectively, and the corresponding annual NEE values were also the highest.

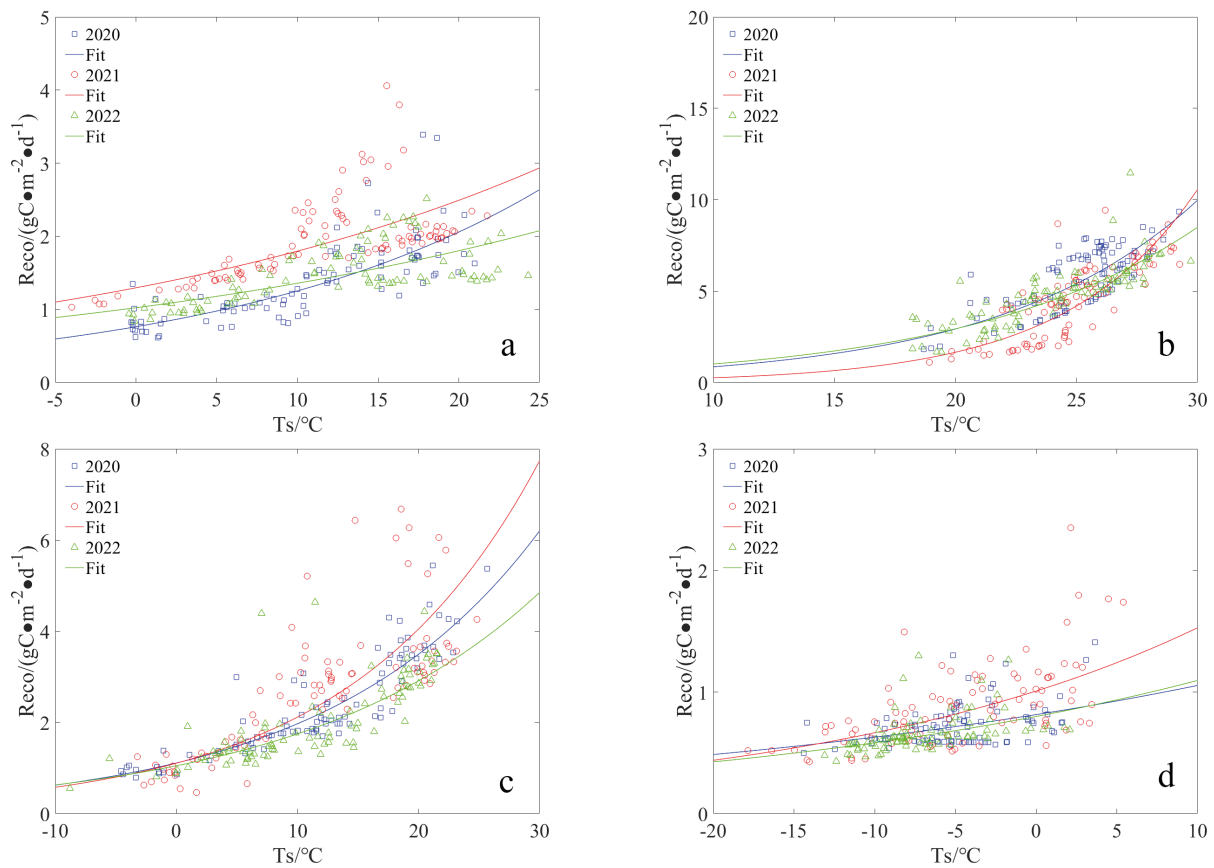


Fig. 9. Relationship between vegetation respiration (Reco: $\text{gC}\cdot\text{m}^{-2}\cdot\text{d}^{-1}$) and soil temperature (T_s : $^{\circ}\text{C}$) in different seasons. The symbols of square, circle, and triangle represent the corresponding values of the two in different years, and the curve represents the exponential relationship fitting between the two. Figures a-d represent spring, summer, autumn, and winter, respectively.

Table 3. Fitting equation and correlation between Reco and soil temperature in each season.

Season	Year	Fitting equation	Correlation	Q_{10}
Spring	2020	$Y=0.7633e^{0.0496x}$	$R^2=0.6924$	1.64
	2021	$Y=1.2961e^{0.0327x}$	$R^2=0.5269$	1.39
	2022	$Y=1.0235e^{0.0283x}$	$R^2=0.5236$	1.33
Summer	2020	$Y=0.2528e^{0.1225x}$	$R^2=0.612$	3.40
	2021	$Y=0.0408e^{0.1852x}$	$R^2=0.6614$	6.37
	2022	$Y=0.3521e^{0.1061x}$	$R^2=0.6943$	2.89
Autumn	2020	$Y=1.1114e^{0.0573x}$	$R^2=0.8547$	1.77
	2021	$Y=1.1075e^{0.0648x}$	$R^2=0.7116$	1.91
	2022	$Y=1.0504e^{0.051x}$	$R^2=0.6994$	1.67
Winter	2020	$Y=0.8149e^{0.0258x}$	$R^2=0.1949$	1.29
	2021	$Y=1.0087e^{0.0416x}$	$R^2=0.4099$	1.52
	2022	$Y=0.7994e^{0.0315x}$	$R^2=0.278$	1.37

Discussion

This study shows a significant correlation between temperature and carbon flux. However, further exploration is needed to establish a quantitative

relationship between temperature and carbon flux. The impact of each meteorological factor on carbon flux was judged separately in the study, but there are also mutual influences and restrictions among meteorological factors. In future studies, it is necessary to further

explore the collaborative impact analysis method among meteorological factors.

This study shows that the greater the variability of crop respiration with soil temperature, the higher the Q_{10} value; at this time, the carbon flux value is also higher. The specific correlation and interaction mechanism among these three factors require further investigation.

Compared to other environmental factors, observing carbon flux changes by eddy covariance systems is highly volatile and unstable, leading to many uncertainties and deviations in both characteristic analysis and correlation analysis. Such deviations become more significant with shorter time scales. The existing methods for processing carbon flux data are insufficient to address many shortcomings, so further improvements and enhancements are needed in the current carbon flux observation, data organization, and processing methods.

The observation station in the text is located in a rice paddy, and there was no drought or water shortage. The study focused on the impact of temperature on crop respiration without considering the influence of soil moisture. Some studies have shown that the impact of water on vegetation respiration is more significant under drought conditions, and even in extreme drought conditions, vegetation respiration may not be affected by temperature [36].

While this study focuses on observations from a single ecological station located in a rice paddy, future research needs to compare observations from rice paddy ecological stations with other types of ecological stations to gain a more comprehensive understanding of carbon flux variations and the impact of environmental factors on carbon flux. This will enhance our understanding of carbon flux variations in larger ecological environments.

In addition to natural environmental factors, urban construction, industrial production, and human activities will also have a significant impact on the carbon cycle. For example, the conversion of natural vegetation into farmland, the emission of pollutants from production and life, and the change of land use patterns, which will directly affect the change in carbon flux. In future research, it is necessary to explore the impact of other factors on the change in carbon flux.

Conclusions

(1) The annual total NEE at the Panjin Ecological Station from 2020 to 2022 was negative, while it was positive during the non-growing season. Among them, the carbon absorption value in 2021 was the largest, reaching $-432.89 \text{ gCm}^{-2}\cdot\text{y}^{-1}$. The heavy precipitation in the early stage and high temperature in the later stage of 2021 are the main reasons for the high carbon absorption value during the growth period of 2021. The diurnal variation of NEE in summer and autumn is characterized by a "high in the middle of the day and low in the morning and evening" pattern, while it is

not obvious in winter and spring. The daily cumulative value of NEE is negative in summer and autumn, with the maximum in summer ranging from -4.28 to $-4.82 \text{ gCm}^{-2}\cdot\text{d}^{-1}$, while it is positive in spring and winter, indicating a carbon source. In spring, the daytime NEE values show significant negative values after late May each year, while the dates for other daytime periods with significant negative values are not fixed. During the summer, the diurnal variation of carbon flux is characterized by a significant negative NEE value during the daytime, peaking at noon and turning positive after sunset. In July, the negative NEE value reaches its maximum, ranging from -20.6 to $-26.0 \mu\text{mol}\cdot\text{m}^{-2}\cdot\text{s}^{-1}$. After mid-October in autumn, there is no longer a significant negative NEE value during the daytime. The annual variation of daily carbon flux is centered around summer, showing a "first increasing and then decreasing" trend. The maximum daily cumulative value occurs in mid to late July, ranging from -11.3 to $-16.0 \text{ gCm}^{-2}\cdot\text{d}^{-1}$.

(2) The impact of precipitation on carbon flux in the early growing season is greater than that of annual precipitation. There is a significant inverse correlation between temperature change and NEE, with high temperatures corresponding to high NEE values. When precipitation and temperature values are high, the specific humidity value is also larger, but sometimes high NEE values occur when the temperature is not high, but the specific humidity is high. The corresponding change law between wind speed and NEE is not significant. The corresponding sunshine value is also high when NEE is high. Temperature, precipitation, sunshine, and specific humidity all promote NEE, with temperature having the most significant impact on NEE changes, followed by precipitation and specific humidity. During the growing season, the NEE value increases significantly with rising temperature, reaching a maximum of $-8.079 \mu\text{mol}\cdot\text{m}^{-2}\cdot\text{s}^{-1}$ when the temperature exceeds 30°C . Especially when the temperature rises by 5°C each time above 15°C , the increment of NEE is similar, approximately $-2.6 \mu\text{mol}\cdot\text{m}^{-2}\cdot\text{s}^{-1}$, showing a clear regularity. During the growing season, when the temperature is below 15°C , it exhibits carbon emissions, while at other temperatures, it exhibits carbon absorption. In the non-growing season, the NEE values corresponding to all temperature ranges are positive, indicating carbon emissions.

(3) The diurnal variation of GPP from June to September was characterized by "high in the middle of the day and low in the morning and evening", with the maximum in July, and the daily cumulative value ranged from 10.69 to $13.55 \text{ gCm}^{-2}\cdot\text{d}^{-1}$. The proportion of GPP in July and August accounts for 52.7 – 60.8% of the annual total. GPP has a significant diurnal variation, reaching its peak at noon. The interannual difference in diurnal variation is most significant in July, with 2021 showing the highest value, corresponding to the highest total GPP in 2021. The annual variation of daily GPP values is centered on summer, showing a pattern of "first increasing and then decreasing". High values occur from

late July to early August, with a maximum of 20.75–23.51 gCm⁻²•d⁻¹. GPP values were low before May 20th and after October 15th.

(4) There is a quadratic polynomial relationship with negative growth between NEE and net radiation from June to September. Among them, the correlation values in July were the highest, with R² exceeding 0.98. Changes in NEE often lag behind those in net radiation. Reco and soil temperature have a clear exponential relationship, with Reco increasing as soil temperature rises. The respiratory intensity is the highest in summer, ranging from 4.54 to 5.68 gCm⁻²•d⁻¹, which is 0.7 to 6.7 times higher than in other seasons, followed by autumn. The variability of crop respiratory intensity with soil temperature in summer is higher than in other seasons, with an increase of 0.71 to 0.85 gCm⁻²•d⁻¹ in respiratory intensity for every 1°C increase in soil temperature. The correlation value between Reco and the soil temperature index fitting is higher in autumn than in other seasons, with the highest value in autumn 2020 (R²=0.85). The higher the variability of Reco with soil temperature, the larger the Q₁₀ value. The Q₁₀ value is the highest in summer, ranging from 2.89 to 6.37, which is 2 to 3 times higher than in other seasons, followed by autumn. The Q₁₀ value in summer and autumn was the highest in 2021, and the corresponding NEE annual value was also the highest.

Acknowledgments

We thank Dr. Jiamin Li of the Department of Atmospheric Sciences, Shenyang Agricultural University, for his helpful revisions of this paper.

Funding

This study was supported by the Joint Open Fund of The Institute of Special Topic of the National Key Research and Development Program of China's Ministry of Science and Technology, Project Approval No.: 2022YFFF0801304; Atmospheric Environment, China Meteorological Administration, Shenyang and Liaoning Provincial Key Laboratory of Agricultural Meteorological Disasters, Project Approval No.: 2023SYIAEFMS18; Shenyang Institute of Atmospheric Environment, China Meteorological Administration, Project Approval No.: 2022SYIAEJY06; Liaoning Provincial Meteorological Bureau of China Project (2025-2026); and the National Natural Science Foundation of China, Project Approval No.: 41975149, 41875157.

Conflict of Interest

The authors declare no conflict of interest.

References

1. IPCC 2021: AR6 Climate Change 2021: The Physical Science Basis, Land Climate, Including Biosphere and Extremes, pp. 48-52, **2021**.
2. HUNG J.K.Y., SCOTT N.A., TREITZ P.M. Drivers of soil nitrogen availability and carbon exchange processes in a High Arctic wetland. *Arctic Science*, **10** (1), 22, **2023**.
3. NISSAN A., ALCOLOMBRI U., PELEG N., GALILI N., JIMENEZ-MARTINEZ J., MOLNAR P., HOLZNER M. Global warming accelerates soil heterotrophic respiration. *Nature Communications*, **14** (1), 3452, **2023**.
4. GEORGIU K., JACKSON R.B., VINDUŠKOVÁ O., ABRAMOFF R.Z., AHLSTRÖM A., FENG W.T., HARDEN J.W., PELLEGRINI A.F.A., POLLEY H.W., SOONG J.L., RILEY W.J., TORN M.S. Global stocks and capacity of mineral-associated soil organic carbon. *Nature Communications*, **13** (1), 3797, **2022**.
5. MA Y.Q., WOOLF D., FAN M.S., QIAO L., LI R., LEHMANN J. Global crop production increase by soil organic carbon. *Nature Geoscience*, **16** (12), 1159, **2023**.
6. NAZIR M.J., LI G.L., NAZIR M.M., ZULFIQAR F., SIDDIQUE K.H.M., IQBAL B., DU D.L. Harnessing soil carbon sequestration to address climate change challenges in agriculture. *Soil and Tillage Research*, **237**, 105959, **2024**.
7. YANG S.S. Study on countermeasures of ecological compensation of wetland in Panjin. Dalian: Dalian University of Technology, China, pp. 15-17, **2019**.
8. SMITH W.K., REED S.C., CLEVELAND C.C., BALLANTYNE A.P., ANDEREGG W.R.L., WIEDER W.R., LIU Y.Y., RUNNING S.W. Large divergence of satellite and Earth system model estimates of global terrestrial CO₂ fertilization. *Nature Climate Change*, **6** (3), 306, **2016**.
9. DESAI A.R., MURPHY B.A., WIESNER S., THOM J., BUTTERWORTH B.J., KOUPEI-ABYAZANI N., MUTTAQIN A., PALERI S., TALIB A., TURNER J., MINEAU J., MERRELLI A., STOY P., DAVIS K. Drivers of decadal carbon fluxes across temperate ecosystems. *Journal of Geophysical Research: Biogeosciences*, **127** (12), 1, **2022**.
10. REED D.E., DUGAN H.A., FLANNERY A.L., DESAI A.R. Carbon sink and source dynamics of a eutrophic deep lake using multiple flux observations over multiple years. *Limnology and Oceanography Letters*, **3** (3), 285, **2018**.
11. SUN S.B., CHE T., LI H.Y., WANG T.J., MA C.F., LIU B., WU Y.T., SONG Z.L. Water and carbon dioxide exchange of an alpine meadow ecosystem in the northeastern Tibetan Plateau is energy-limited. *Agricultural and Forest Meteorology*, **275**, 283, **2019**.
12. WANG Y.Y., ZHU Z.K., MA Y.M., YUAN L. Carbon and water fluxes in an alpine steppe ecosystem in the NamCo area of the Tibetan Plateau during two years with contrasting amounts of precipitation. *International Journal of Biometeorology*, **64** (7), 1183, **2020**.
13. ZHAN Y.L., DENG Y.B., WANG J., LIU Q., WANG W.M. Environmental response characteristics of the carbon and water fluxes above complex urban surfaces of a subtropical megacity in China. *Physics and Chemistry of the Earth*, **135**, 103681, **2024**.
14. GAO Y., OUYANG Z.T., SHAO C.L., CHU H.S., SU Y., GUO H.Q., CHEN J.Q., ZHAO B. Field observation of lateral detritus carbon flux in a coastal wetland. *Wetlands*,

- 38**, 613, **2018**.
15. XU C.H., MAO F.J., DU H.Q., LI X.J., SUN J.Q., YE F.F., ZHENG Z.D., TENG X.F., YANG N.X. Full phenology cycle carbon flux dynamics and driving mechanism of Moso bamboo forest. *Frontiers in Plant Science*, **15**, 1359265, **2024**.
 16. ZAHN E., GHANNAM K., CHAMECKI M., MOENE A.F., KUSTAS W.P., GOOD S., BOU-ZEID E. Numerical investigation of observational flux partitioning methods for water vapor and carbon dioxide. *Journal of Geophysical Research: Biogeosciences*, **129** (6), 1, **2024**.
 17. WAGLE P., GOWDA P.H., NORTHUP B.K., TURNER K.E., NEEL J.P.S., MANJUNATHA P., ZHOU Y.T. Variability in carbon dioxide fluxes among six winter wheat paddocks managed under different tillage and grazing practices. *Atmospheric Environment*, **185** (7), 100, **2018**.
 18. WANG J., FENG L., PALMER P.I., LIU Y., FANG S.X., BÖSCH H., O'DELL C.W., TANG X.P., YANG D.X., LIU L.X., XIA C.Z. Large Chinese land carbon sink estimated from atmospheric carbon dioxide data. *Nature*, **586**, 720, **2020**.
 19. FELDMAN A.F., ZHANG Z., YOSHIDA Y., CHATTERJEE A., POULTER B. Using Orbiting Carbon Observatory-2 (OCO-2) column CO₂ retrievals to rapidly detect and estimate biospheric surface carbon flux anomalies. *Atmospheric Chemistry and Physics*, **23** (2), 1545, **2023**.
 20. LV Y.P., GU L.H., XU J.Z., LIU X.Y. A coupled hourly water-carbon flux model at plot and field scales for water-saving irrigated rice paddy. *Agricultural Water Management*, **293**, 108706, **2024**.
 21. JUHÁSZ C., HUZSVAI L., KOVÁCS E., KOVÁCS G., TUBA G., SINKA L., ZSEMBELI J. Carbon Dioxide Efflux of Bare Soil as a Function of Soil Temperature and Moisture Content under Weather Conditions of Warm, Temperate, Dry Climate Zone. *Agronomy*, **12** (12), 1, **2022**.
 22. KUMAR A.N., BHATIA A., FAGODIYA R.K., MALYAN S.K., MEENA B.L. Eddy covariance flux tower: a promising technique for greenhouse gases measurement. *Advances in Plants and Agriculture Research*, **7** (4), 337, **2017**.
 23. ZHANG M.L., ZHOU L., ZHOU G.S. Climate warming and changes in precipitation distribution lead to early maturity and increased yield of rice in Panjin. *China Rice*, **27** (3), 51, **2021**.
 24. LIU G.F., WANG N., YOU M., WANG Y. Analysis on climate characteristics and changes of Panjin City from 1981 to 2010. *Agriculture of Jilin*, **9**, 103, **2018**.
 25. ZHANG K.D., GONG Y., FA H., ZHAO M. Co₂ flux characteristics of different plant communities in a subtropical urban ecosystem. *Sustainability*, **11** (18), 4879, **2019**.
 26. NIU S.L., CHEN W.N., LIÁNG L.L., SIERRA C.A., XIA J.Y., WANG S., HESKEL M., PATEL K.F., BOND-LAMBERTY B., WANG J.S., YVON-DUROCHER G., KIRSCHBAUM M.U.F., ATKIN O.K., HUANG Y.Y., YU G.R., LUO Y.Q. Temperature responses of ecosystem respiration. *Nature Reviews Earth and Environment*, **5** (8), 559, **2024**.
 27. FENG J.G., WANG J.S., SONG Y.J., ZHU B. Patterns of soil respiration and its temperature sensitivity in grassland ecosystems across China. *Biogeosciences*, **15**, 5329, **2018**.
 28. FATIMA Z., AHMED M., HUSSAIN M., ABBAS G., UL-ALLAH S., AHMAD S., AHMED N., ALI M.A., SARWAR G., HAQUE E.U., IQBAL P., HUSSAIN S. The fingerprints of climate warming on cereal crops phenology and adaptation options. *Scientific Reports*, **10** (1), 18013, **2020**.
 29. HU T.X., ZHANG X.S., KHANAL S., WILSON R., LENG G.Y., TOMAN E.M., WANG X.H., LI Y., ZHAO K.G. Climate change impacts on crop yields: A review of empirical findings, statistical crop models, and machine learning methods. *Environmental Modelling and Software*, **179**, 106119, **2024**.
 30. YANG P., ZHAO L.Q., LIANG X.R., NIU Z.M., ZHAO H., WANG Y.Y., WANG N.A. Response of net ecosystem CO₂ exchange to precipitation events in the Badain Jaran Desert. *Environmental Science and Pollution Research*, **29** (24), 36486, **2022**.
 31. ZHANG R., ZHAO X.Y., ZUO X.A., QU H., DEGEN A.A., LUO Y.Y., MA X.J., CHEN M., LIU L.X., CHEN J.L. Impacts of precipitation on ecosystem carbon fluxes in desert-grasslands in Inner Mongolia, China. *Journal of Geophysical Research: Atmospheres*, **124** (3), 1266, **2019**.
 32. CROUS K.Y., UDDLING J., KAUWE M.G.D. Temperature responses of photosynthesis and respiration in evergreen trees from boreal to tropical latitudes. *New Phytologist*, **234** (2), 353, **2022**.
 33. WANG C., MORRISSEY E.M., MAU R.L., HAYER M., PIÑEIRO J., MACK M.C., MARKS J.C., BELL S.L., MILLER S.N., SCHWARTZ E., DIJKSTRA P., KOCH B.J., STONE B.W., PURCELL A.M., BLAZEWCZ S.J., HOFMOCKEL K.S., PETT-RIDGE J., HUNGATE B.A. The temperature sensitivity of soil: microbial biodiversity, growth, and carbon mineralization. *The ISME Journal*, **15** (9), 2738, **2021**.
 34. MEYER N., WELP G., AMELUNG W. The temperature sensitivity (Q₁₀) of soil respiration: controlling factors and spatial prediction at regional scale based on environmental soil classes. *Global Biogeochemical Cycles*, **32** (2), 306, **2018**.
 35. HAAF D., SIX J., DOETTERL S. Global patterns of geoeological controls on the response of soil respiration to warming. *Nature Climate Change*, **11** (7), 623, **2021**.
 36. YAO J.Y., GAO Z.M., HUANG J.P., LIU H.P. Uncertainties in eddy covariance CO₂ fluxes in a semiarid sagebrush ecosystem caused by gap-filling approaches. *Atmospheric Chemistry and Physics*, **21**, 15589, **2021**.